Cancellous Bone Histomorphometry and Fractal Analysis: Automated Skeletonization for Quantitative Assessment of Trabecular Connectivity and Complexity

HU Revista
Artigo Original

Histomorfometria Óssea e Análise Fractal: Esqueletonização automatizada objetivando avaliação da conectividade trabecular e sua complexidade

Thiago Pires Claudio[1]
Daniela Oldra Zanotto[1]
Matheus de Abreu[2]
Riéli Elis Schulz[1]
Daniel Caye[1]
Rogério Oliveira Gondak[3]
Gustavo Davi Rabelo[1]

[1]Federal University of Santa Catarina (Department of Dentistry), Florianópolis, Santa Catarina, Brazil.

[2]A.C. Camargo Cancer Center (Department of Epidemiology), São Paulo, São Paulo, Brazil.

[3]Federal University of Santa Catarina (Department of Pathology), Florianópolis, Santa Catarina, Brazil.

✉ **Gustavo Rabelo**

Endereço: : R. Rui Delfino Conti, 275, Trindade, Florianópolis, SC.
CEP: 88040-900
gustavo.rabelo@ufsc.br

Submetido: 18/10/2025
Aceito: 06/03/2026

ABSTRACT

Introduction: Bone trabeculae complexity can be assessed in histology through skeletonization by measuring structural parameters and fractal analysis. **Objective:** To develop computational codes for automated bone trabeculae skeletonization in histological images to extract trabeculae data and Fractal Dimension (FD). **Material and Methods:** Cancellous bone from healthy (HB) and pathological (PB) conditions were analyzed in Mallory trichrome (MT) and hematoxylin & eosin (H&E) stained histological sections. Digital images (10× magnification) included MT staining with HB (n=26) and PB (n=147) and H&E staining with HB (n=55) and PB (n=46). Computational codes were created to automate segmentation and skeletonization using thresholding binarization. MT code involved color splitting channels, while H&E code used automatic thresholding. Skeletonized structures were analyzed for the number of trabeculae (Tb.n), branches (Brch), junctions (Jc), and endpoints (End.P). FD was determined via box-counting. **Results:** Both computational codes retrieved a well-defined skeletonized structure representing the trabecula in all images. Excellent visual matching of the linear structure compared with the original image for both HB and PB were found. Tb.n was higher for PB in both conditions and stains analyzed (p=0.0001). FD for PB was lower than HB (p=0.02) only in the H&E staining. In the four situations analyzed, FD showed strong positive correlations with Brch and Jc and moderate negative correlations with Tb.n and End.P (p<0.05). **Conclusion:** Automated skeletonization was achieved using computational codes to assess trabeculae spatial organization, including fractal analysis. PB and HB differed in Tb.n and FD, which correlated with all microarchitectural parameters.

Keywords: Bone and Bones; Bone diseases; Cancellous Bone, Histology, Fractals.

RESUMO

Introdução: A complexidade das trabéculas ósseas pode ser avaliada histologicamente pela esqueletonização por meio de parâmetros estruturais e análise fractal. **Objetivo:** Desenvolver códigos computacionais para automatização da esqueletonização das trabéculas ósseas em imagens histológicas com a finalidade de extrair dados da organização trabecular e dimensão fractal (FD). **Material e Métodos:** Cortes histológicos de osso esponjoso provenientes de condições saudáveis (HB) e patológicas (PB) foram corados por tricrômico de Mallory (MT) e hematoxilina-eosina (H&E) e imagens digitais (ampliação de 10×) foram avaliadas: MT tinha HB (n=26) e PB (n=147), e H&E com HB (n=55) e PB (n=46). Os códigos computacionais foram criados com comandos para automatizar a segmentação e a esqueletonização por meio de thresholding. O código para MT envolveu a separação de canais de cor, enquanto o de H&E utilizou thresholding automático. As estruturas esqueletonizadas foram analisadas quanto ao número de trabéculas (Tb.n), ramificações (Brch), junções (Jc) e pontos terminais (End.P). A FD foi determinada pelo método de box-counting. **Resultados:** Em todas as imagens, os códigos computacionais resultaram em uma estrutura esqueletonizada bem definida, representando adequadamente as trabéculas. Houve excelente correspondência visual entre as estruturas lineares esqueletonizadas e as imagens originais, tanto em HB quanto em PB. O número de trabéculas (Tb.n) foi maior em PB em ambas as condições e colorações analisadas (p=0,0001). A FD foi menor em PB do que em HB (p=0,02) apenas na coloração por H&E. Nas quatro situações avaliadas, a FD apresentou forte correlação positiva com Brch e Jc, e correlação negativa moderada com Tb.n e End.P (p<0,05). **Conclusão:** A esqueletonização automatizada foi obtida com sucesso por meio de códigos computacionais, permitindo avaliar a organização espacial das trabéculas, incluindo a análise fractal. HB e PB diferiram em relação a Tb.n e FD, que apresentaram correlações significativas com todos os parâmetros microestruturais

Palavras-chave: Osso e Ossos; Doenças Ósseas; Osso Esponjoso; Histologia, Fractais.

INTRODUCTION

Despite advances in non-invasive imaging techniques, bone histomorphometry remains the best method for examining bone tissue and cellular components.[1] Static and dynamic bone histomorphometry analysis require repetitive tasks, which are time-consuming, and computer-assisted approaches have been proposed to improve efficiency, reproducibility of the process and reduce time-consuming.[2,3]

In histological evaluation, the assessment of the trabecular network is fundamental to understanding bone behavior under physiological and pathological conditions. Skeletonization of histological images enables the evaluation of trabecular organization by converting each trabecula into a simplified linear representation in a binary image. This transformation allows quantification of the topographical and geometric characteristics of trabecular junctions and branches.[4,5]

Skeletonization and its analysis are extensively used in radiographic images to evaluate the cancellous bone, mostly followed by fractal analysis.[6,7] Fractal Dimension (FD) in fractal analysis indicates the complexity of the spatial organization of the bone structure.[8,9] As in radiographic images, and in histological slides, the trabecular bone has two-dimensional (2D) fractal characteristics, which can be evaluated and correlated with biomechanical properties. A single fractal dimension is insufficient to replace classic 2D descriptors of microarchitecture, but it can add information as it can reflect the complexity of branching trabeculae.[10,11] In pathology and histology, fractal analysis techniques for characterizing cells and tissues can support differential diagnosis between pathological and healthy conditions.[12]

Beyond analyzing trabeculae, branches, and junctions, exploring their association with FD may enhance cancellous bone assessment through histomorphometry. The key question is whether FD analysis of histological images can distinguish healthy bone (HB) from pathological bone (PB), as shown in radiographic studies. If FD can differentiate osteoporotic from normal bone, it may also detect subtler alterations in other bone diseases or conditions. Moreover, the creation of an automated algorism through computational codes could significantly reduce analysis time and improve reproducibility in bone research. The addition of one index in the bone evaluation could add value to bone research once it goes beyond the classical quantitative parameters.

Therefore, the aim of this study was to develop and test automated computational codes for skeletonization of histological bone images, enabling a quantitative approach of the evaluation of the trabecular organization through fractal analysis, also to investigate whether this index would be useful in differentiating healthy from pathological bone.

MATERIAL AND METHODS

Study design and sample selection

A retrospective cross-sectional study was conducted using samples from the Biobank of the Oral Pathology Laboratory (Biobank registration: CONEP B-051) and a control group from previous study (approved by the Research Ethics Committee of the Federal University of Santa Catarina, CAAE No 28234620.0.0000.0121, approval number 4.063.334). Informed consent was obtained from all donors. Patient identities remained anonymous in accordance with the Declaration of Helsinki.

The study aimed to develop and apply automated computational codes for histological trabecular complexity analysis. Therefore, the sample size and inclusion criteria were defined based on the availability of material suitable for the histological images acquisition and processing. Healthy bone (HB) was collected from the disease-free surgical margins of resected mandibles from patients with oral squamous cell carcinoma (OSSC) (n=10). These samples were stained both in hematoxylin and eosin (H&E) and Mallory's Trichrome (MT) to compose the HB group. Pathological bones (PB) samples were obtained in two distinct conditions: 1) in the bone/tumor interface of resected mandibles of the same patients with OSSC in the HB group (n=10) with proven mandibular invasion, with the histological sections stained in H&E, and 2) in lesional bone from benign fibro-osseous lesions of fibrous dysplasia affecting the jaws (BFOLs, n=10), stained in MT.

A qualitative analysis was conducted to confirm the presence of bone components (cortical, trabecular/cancellous, and osteoid) and to identify cancellous bone, including trabeculae and branches. Only lamellar bone with intact trabeculae was analyzed.

A total of 120 histological slides from 20 patients were selected (including 20 HB and 100 PB — 40 from the tumor/bone interface and 60 from fibrous dysplasia). Digital images of cancellous bone were obtained as much as was needed to develop the computational codes for bone histomorphometry, assessing trabecular skeleton properties and FD.

Histopathological processing and skeletonization

These histological sections were obtained with 3 µm thickness. The initial evaluation was performed on MT-stained histological sections, as this staining process provides mature and lamellar bone tissue predominantly in red. The histological slides were scanned using ScanScope AT equipment. The images were analyzed using Aperio ImageScope software (Version 12.4.3.5008,

Leica Biosystems).

In each histological section, all areas matching with trabecular/cancellous bone were selected, and photographs were captured until covering all areas containing the bone trabeculae using an original 10x magnification. Each image captured was defined as a region of interest (ROI). The number of ROIs per slide varied from 3 to 15 depending on the amount of bone material collected during the biopsy procedure. Samples with less material or fewer bone components were fully covered with around 3 images. For MT, ROIs with a mixed color (red and blue) were excluded from the analysis.

Skeletonization was performed automatically by creating computational codes for ImageJ/Fiji (1.54, Wayne Rasband and contributors, National Institutes of Health, USA) using the macro recording function when testing different image processing tasks. The commands were inserted in the computational code (Appendix A) designed to run based on the predominant color in the images, which was red.

Several tests were conducted based on the binarization process and the visual result of the trabeculae representation. The following steps resulted in the skeletonized image: after splitting the color channels, the code renders the mature lamellar bone in red by selecting the blue channel. A fixed threshold value was selected after several tests conducted by the research team to retrieve the most representative skeleton line of the trabeculae. The skeletonized structure was analyzed using the BoneJ plugin,[13] selecting both options for each image, the cycle pruning method defined as "none" and the option "Prune ends" (meaning prune any branch that ends in an endpoint), and clicking the ok button. The skeleton was analyzed considering the number of trabeculae (Tb.n), number of branches (Brch), number of junctions (Jc), and number of endpoints (End.P).

The computational code included the command for FD analysis using the tool "Fractal Box Count" in ImageJ/Fiji, with box sizes of 2, 3, 4, 6, 8, 12, 16, 32, and 64. The code was designed to open the results window automatically together with the summary of the skeleton analysis after running. FD is represented by the letter D in the last column. The automated commands render the entire folder containing the images and generate a new output folder with all the skeletonized images.

After creating the first computational code, similar commands were used to create a new code for H&E-stained histological sections. Although, since H&E staining has no higher contrast compared to MT staining, several thresholding options and other image-processing tools were assessed to enhance the skeletonization process. The command list of this second code included: Enhanced contrast with equalization, Maximum filter application, and automatic thresholding using the default configuration. This computational code was named H&E code (Appendix B), and like the MT code, it included both functions for analyzing the skeleton and obtaining the FD value in each image. The results were extracted from the results and summary files for statistics of groups comparison and correlation analysis.

Statistical analysis

Values are presented as the median and interquartile range (IQR, 25th-75th percentile) in the text and tables. The Shapiro-Wilk test was used to assess the normal distribution of data. Groups were compared using the Mann-Whitney U non-parametric statistical test. Spearman's correlation test was applied to analyze relationships between quantitative trabecular microarchitecture data and FD, with a correlation coefficient classified as very strong (>0.9), strong (0.7–0.89), moderate (0.4–0.69), and weak (<0.39).[14] A significant level of 5% was considered. Multiples ROIs obtained from the same patient were included in the analysis and treated as individual observation. Statistical analyses were conducted using GraphPad Prism 9 (La Jolla, California, USA).

RESULTS

We analyzed 173 digital images using the MT code (HB: n=26, PB: n=147) and 101 images using the H&E code (HB: n=55, PB: n=46). A qualitative visual matching analysis revealed that the two computational codes effectively retrieved the skeletonized structure from the histological images. All the skeletonized structures for each image were visually compatible with the trabeculae within the image (Figure 1). The final best version of the two codes were then defined, as follows: MT code focused on splitting the image channels and applied a fixed threshold, followed by removing outliers, filling the holes, and using a Gaussian blur filter before binarization and skeletonization, and the H&E code included the enhanced contrast with equalization and applied a maximum filter and binarization. Outliers' removal and the step of filling the holes after binarization using the default option from the ImageJ/Fiji software were the commands tested which retrieved the best visual results.

Both codes were developed to run in batch mode on all images within a folder and successfully retrieved the trabecular connectivity parameters together with FD values.

A pipeline of the developed codes is described in Figure 2.

Regarding trabecular connectivity parameters, Tb.n was higher for PB in both conditions and stains analyzed (p=0.0001). FD in PB was lower than in HB (p=0.02) only in H&E staining. In the four situations analyzed, FD showed strong positive correlations with Brch and Jc and moderate negative correlations with Tb.n

and End.P ($p<0.05$). Tables 1 and 2 present the skeleton junction, connection analysis, and FD measurements. Table 1 compares HB and PB, and Table 2 compares HB stained in MT and H&E using two computational codes.

The correlation between connectivity parameters and fractal dimension (FD) confirmed that FD is associated with trabecular microarchitectural features; however, stronger correlations were observed only for connection-related parameters, not for the number of trabeculae (Table 3).

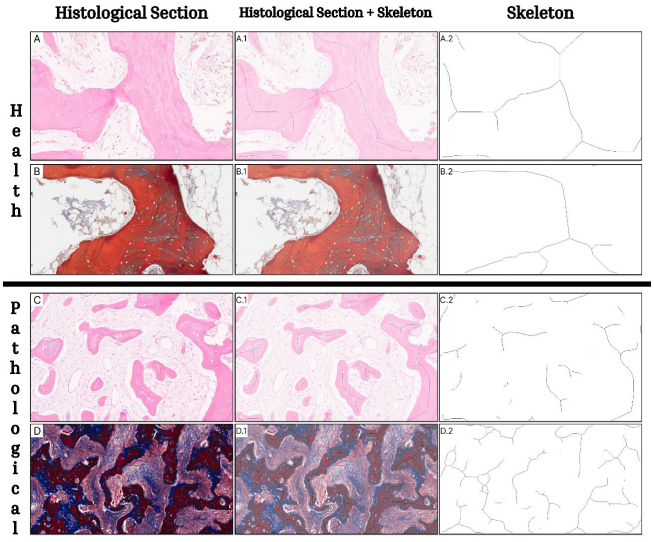

Figure 1: Comparison of histological sections of health and pathological bone and their skeletonized representation.

Legend: (A, B) Histological sections of health bone tissue stained with Hematoxylin & Eosin (A) and Mallory's Trichrome (B). Same image with overlaid skeletonized structure (A.1, B.1). Skeletonized structure of the health bone trabeculae (A.2, B.2). (C, D) Histological sections of pathological bone tissue stained with Hematoxylin & Eosin (C) and Mallory's Trichrome (D). Same image overlaid its respective skeletonized structure (C.1, D.1). Skeletonization of the pathological bone trabeculae (C.2, D.2).

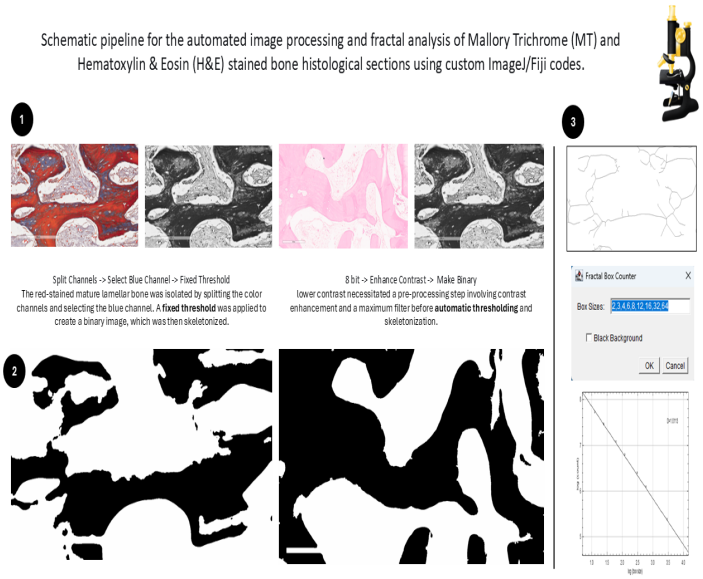

Figure 2: Automated image analysis pipeline.

Legend: Histological slides of bone were imaged at 10x magnification to capture all trabecular bone areas as Regions of Interest (ROIs). Two independent computational codes were developed for ImageJ/Fiji to process images based on their staining. 1) First steps of image processing are included in both codes to promote the transformation of the original images through several processes until having the best binary image for skeletonization. 2) Binary images before skeletonization. 3) The skeletonized image and the FD analysis using "Fractal Box Counter" tool and the resulted plot including FD value on the upper corner.

Table 1: Comparison between healthy and pathological bone considering the two stains used in the study.

Parameters	MT			H&E		
	HB	PB	p-value	HB	PB	p-value
Tb.n (n)	5 (3; 9.2)	13.5 (8.7; 21.7)	0.0001	5 (2; 7)	8 (5; 11.2)	0.0001
Brch (n)	3.67 (2.18; 5.22)	4.08 (2.47; 5.27)	0.61	3 (2; 4.85)	2.74 (2.24; 3.7)	0.75
Jc (n)	1.45 (0.69; 2.02)	1.58 (0.75; 2.28)	0.63	1 (0.5; 2)	0.87 (0.6; 1.37)	0.70
End.P (n)	0.5 (0.38; 0.67)	0.61 (0.5; 0.67)	0.11	0.57 (0.42; 0.71)	0.65 (0.5; 0.71)	0.22
FD (#)	0.95 (0.94; 0.96)	0.96 (0.94; 0.98)	0.37	0.96 (0.95; 0.97)	0.95 (0.92; 0.96)	0.02

Legend: Median and interquartile range (IQR). Mann-Whitney test. Significant differences $p<0.05$ in bold. MT Mallory Trichrome, H&E Hematoxylin & Eosin, HB Health Bone, PB Pathological Bone. Tb.n trabeulcar number, Brch.n branch number, Jc junction number, End.P number of endpoints, FD fractal dimension.

Table 2: Comparison of cancellous healthy bone stained with two different stains and evaluated with distinct computational codes.

Parameters	MT	H&E	p-value
Tb.n (n)	5 (3; 9.2)	5 (2; 7)	0.66
Brch (n)	3.67 (2.18; 5.22)	3 (2; 4.85)	0.30
Jc (n)	1.45 (0.69; 2.02)	1 (0.5; 2)	0.26
End.P (n)	0.5 (0.38; 0.67)	0.57 (0.42; 0.71)	0.42
FD (#)	0.95 (0.94; 0.96)	0.96 (0.95; 0.97)	0.75

Legend: Median and interquartile range (IQR). Mann-Whitney test. Significant differences p<0.05. MT Mallory Trichrome, H&E Hematoxylin & Eosin, Tb.n Trabecular number, Brch Branches, Jc Junctions, End.P End-points, FD Fractal Dimension.

Table 3: Correlation between FD and trabecular microarchitecture parameters for both healthy and pathological bone with different stains and analyzed trough different codes.

		Tb.n	Brch	Jc	End.P
MT HB	FD	r -0.53 p 0.007	r 0.82 p<0.0001	r 0.82 p<0.0001	r -0.54 p 0.004
MT PB		r -0.19 p 0.28	r 0.96 p<0.0001	r 0.96 p<0.0001	r -0.54 p 0.001
H&E HB		r -0.62 p <0.0001	r 0.71 p<0.0001	r 0.71 p<0.0001	r -0.54 p<0.0001
H&E PB		r -0.64 p<0.0001	r 0.86 p<0.0001	r 0.86 p<0.0001	r -0.27 p 0.06

Legend: Spearman test and correlation coefficient (rs). Values in bold represent a strong or very strong correlation. MT Mallory Trichrome, H&E Hematoxylin & Eosin, HB Health Bone, PB Pathological Bone, Tb.n Trabecular number, Brch Branches, Jc Junctions, End.P End-points, FD Fractal Dimension.

DISCUSSION

Skeletonization proved to be an effective approach for representing the spatial distribution of bone trabeculae in histological images. This linear representation of trabecular connectivity enabled the evaluation of connection-related parameters and, additionally, the assessment of structural complexity through fractal dimension analysis. Trabecular connectivity and complexity were found to be correlated, revealing that these features can be quantified in two-dimensional histological images by extracting the linear representation of trabeculae and their interconnections.

The skeletonized structures accurately reflected the trabecular branches and junctions, maintaining close alignment with the original bone architecture. The validation of the skeletonization process in computational vision is inherently visual. There are no alternative quantitative tools to confirm the transformation of a trabecular network into its linear skeleton in a 2D histological section. While such quantitative validation is possible in 3D analyses (e.g., micro-CT), the primary aim of this study was to introduce a novel index (fractal dimension) for future applications in routine 2D analyses, such as conventional histomorphometry and pathological anatomy, where visual confirmation remains the established standard, although also in the need of other studies and validation. Despite minor discrepancies in a few images, the skeletonization process effectively highlighted the intricate trabecular network, enabling the assessment of both conventional connectivity parameters and FD.

Among the trabecular characteristics, Tb.n was the only parameter that differed when comparing distinct conditions (PB X HB), it may reinforce the limitation of 2D histological analysis in the full complexity of trabecular connectivity. In our case, two PB conditions, with two HB conditions. One of the PB condition was a cancellous bone within fibrous dysplasia, a condition characterized by substituting the normal bone to a fibrous tissue with immature and disorganized bone formation. The other PB condition was the lamellar cancellous bone adjacent to the island and nests of oral squamous cell carcinoma, which appears remodeled due to bone invasion. Although biologically different, both conditions induce remodeling processes, potentially explaining the increase of trabeculae (Tb.n). However, there were no differences in Brch and Jc. One could assume that remodeling processes in PB conditions may interfere with Tb.n or their format since we assessed their microarchitecture in 2D images. Considering the medullary spaces and the trabecular thickness variations in our images, our qualitative analysis indicated that the skeletonized structure accurately represented the trabecular structure. HB is expected to differ from PB conditions.

In addition to evaluating trabecular microarchitecture, the computational codes incorporated FD measurement to enhance histological analysis. Significant differences in FD between HB and PB were observed only in H&E-stained sections. In MT-stained images, the bone component was largely embedded within a fibrous lesion, which may have limited FD differentiation. In the H&E staining, both HB and PB showed lamellar and morphologically normal bone; however, the PB samples were affected by tumor invasion and active remodeling in the surrounding tissue. The lower FD observed in PB indicates that spatial organization of trabeculae differed from HB, even when both appeared structurally intact—unlike in osteoporosis, where trabeculae are thinner and less connected, for example. These findings suggest that FD can distinguish HB from PB, even in cases with subtle architectural alterations. Consistent with our results, previous studies have also demonstrated that FD can differentiate pathological from non-pathological bone, including analyses based on radiographic images, which rely on lower resolution than histological sections.[7,15]

Considering the FD difference in the H&E-staining, we can suggest that the computational code including skeletonization and binarization after equalization and using a default threshold option may be the optimal situation to differentiate cancellous bone in distinct conditions using organization complexity assessment. This complexity assessment is supported by calculating FD. In studies on the fractal properties of bone[9], although focused only on radiographic findings, experimental conditions determining the fenestration of trabecular plates and the loss of entire trabecular branches may influence the divergences among studies using FD. This dependence of FD on trabecular branches found in radiology studies may also apply to microscopy images.

At the same time, we assume that this problem could be controlled for histology, since the higher resolution of the trabeculae is one advantage of using microscopy images to show their branches. However, it may not represent their real connections since it is a 2D image. Despite this limitation, other situations in microscopy showed that FD accurately represented microarchitecture. A previous study conducted by our research group demonstrated FD as a key tool for analyzing cortical bone canal distribution,[16] meaning that FD can be implemented when analyzing bone complexity, and this parameter should be associated with other microarchitecture parameters to retrieve robust evaluation of bone structure. The present study extends its usefulness to a cancellous bone analysis by showing different significances comparing HB and PB conditions.

Moreover, our results revealed that FD correlated with the trabecular microarchitectural parameters. The strong and positive correlations between FD and connectivity-related parameters suggest that FD primarily reflects the intricacy and interlinking of the trabecular network rather than the mere number of trabeculae. While trabecular number quantifies the elements within the structure, FD captures the overall spatial complexity and branching patterns that define connectivity.

One thing to take care of is that FD may be misinterpreted when analyzed by itself as an only individual parameter. As FD was correlated with connection-related parameter, our computational code included these microarchitectural parameters to be always interpreted together. Chappard et al. (2008)[17] described that FD can be measured by the box-counting method, which involves superimposing a series of grids of equally sized squares over an image of the trabecular boundaries, or other methods. They also reported that none of the methods are mutually exclusive, and none provides a unique parameter that fully describes microarchitecture, which we agree with and was one reason to use the skeletonized structure to be fully evaluated.

Still on correlation, FD showed a positive correlation with Brch and Jc and a negative correlation with Tb.n and End.P. These correlations occurred in the four conditions analyzed, two of them in PB condition. Hence, regardless of HB or PB condition of the cancellous bone, FD increased when Brch and Jc increased, and FD decreased when Tb.n and End.P increased. As FD is related to bone distribution and organization within its own space, this seems more associated with branches and interconnections than Tb.n. These correlations between FD and trabeculae parameters bring new information since literature fails to evaluate these associations. A study conducted in an experimental model showed a correlation between the number of osteoclasts and the FD in histological sections, calculating FD on the binarized image of the bone surface.[18] In the end, as FD is correlated with other bone parameters assessed in histology, this could encourage bone researchers to include this index in their future studies.

Beyond using computational codes to evaluate microarchitecture and FD, automated workflows can significantly promote data for bone research by reducing time when used in multiple images. In our study, we automated the skeletonization process and developed two computational codes for bone histomorphometry images from two distinct stains. Automated analysis is a faster and less time-consuming approach and may improve reproducibility, it should be encouraged in research focused on developing computational codes as it is easy to install and use. Using codes in globally established open-source platforms such as ImageJ/Fiji is important and democratic. Previous studies have demonstrated favorable application of automated and

semi-automated methods for bone evaluation through open-source software for bone histomorphometry analysis.[19,20] Beyond using easy to access software, skeletonization can also be encouraged because they are easy to be performed with tools and plugins in software such as the ImageJ/Fiji. A previous study from our group used skeletonization to compare diabetic and non-diabetic trabecular bone microarchitecture in an experimental model[21], although not in an automated manner, which limited the inclusion of a larger number of images in the dataset.

When considering automation and time-consuming, Linhares et al[3] conducted a study on bone evaluation by histological images. They developed an automated evaluation code of the bone matrix, concluding that the automatic approach was highly accurate and significantly shortened the time required compared with the manual method. In this study, global thresholding enabled automation of the image processing pipeline, with adjustments made according to the staining characteristics. To our knowledge, this is the first study to apply skeletonization for assessing bone distribution in pathological conditions such as fibrous dysplasia and at the bone–tumor interface. The inclusion of FD analysis further allowed the evaluation of cancellous bone organization under disease-related imbalance. Overall, the skeletonization process effectively quantified trabecular branches and junctions, demonstrating their association with the spatial distribution of bone trabeculae.

The present study has limitations. The analysis was restricted to 2D histological sections, limiting the assessment of 3D trabecular connectivity. The small cohort of HB when compared to PB, and the PB conditions of the samples comprised different biological conditions and the age distributions (patients with fibrous dysplasia tend to be younger and patients with oral cancer tend to be older). Also, MT staining, which was particularly complex and challenging due to the color heterogeneity. Therefore, we had to refine the computational codes to improve the quality of the segmentation process. From a practical perspective, we believe that the limitations mentioned are not relevant when considering our main goal, which was to create computational codes for bone histomorphometry associated with FD analysis, that add value to bone analysis, and to inform that this could be performed in open-source software for all researchers worldwide.

CONCLUSION

Fractal dimension (FD) derived from bone trabeculae skeletonization provides a valid composite index of cancellous microarchitecture, reflecting structural complexity and connectivity as demonstrated by its positive correlation with branch and junction counts and negative correlation with trabecular number and endpoints. Therefore, FD should be interpreted alongside standard morphometric parameters. The automated computational codes developed in this study enable reproducible skeletonization and fractal analysis of both MT and H&E-stained sections through robust color segmentation and image processing. This automated approach represents a promising tool to enhance efficiency and standardization in cancellous bone histomorphometry.

FUNDING

The research leading to these results received funding from the National Council for Scientific and Technological Development (CNPq) under grant agreement number 403656/2021-4. The author TPC thanks Coordination for the Improvement of Higher Education Personnel (CAPES) [Finance Code 001]. The author RES thanks the Foundation for Research and Innovation of the State of Santa Catarina (FAPESC).

ACKNOWLEDGMENTS

The authors thank Prof. Paula Dechichi of the Federal University of Uberlândia for scientific support and the Multiuser Laboratory of Biology Studies (LAMEB/UFSC) for providing the facilities for microscopy analysis.

ETHICAL APPROVAL

Ethical approval was waived by the local Research Ethics Committee of the Federal University of Santa Catarina (CAAE No. 28234620.0.0000.0121, approval number 4.063.334).

DECLARATION OF GENERATIVE AI AND AI-ASSISTED TECHNOLOGIES IN THE WRITING PROCESS

During the preparation of this work, the authors used ChatGPT (https://chatgpt.com/) and DeepSeek (https://chat.deepseek.com/) to assist with text editing and H&E computational code creation. After using this tool, the authors carefully reviewed and edited the content as needed and took full responsibility for the final publication.

CONFLICT OF INTEREST

The authors declare no conflicts of interest relevant to the content of this article.

REFERENCES

1. Chavassieux P, Chapurlat R. Interest of Bone Histomorphometry in Bone Pathophysiology Investigation: Foundation, Present, and Future. Front Endocrinol (Lausanne) 2022; 13; DOI: 10.3389/FENDO.2022.907914.

2. Brent MB, Emmanuel T. Contemporary Advances in Computer-Assisted Bone Histomorphometry and Identification of Bone Cells in Culture. Calcif Tissue Int 2023; 112(1):1–12; DOI: 10.1007/s00223-022-01035-2.

3. Linhares CRB, Rabelo GD, Limirio PHJO, Venâncio JF, Silva IGR, Dechichi P. Automated bone healing evaluation: New approach to histomorphometric analysis. Microsc Res Tech 2022; DOI: 10.1002/JEMT.24188.

4. Saha PK. Characterization of trabecular bone plate–rod micro-architecture using skeletonization and digital topologic and geometric analysis. Skeletonization: Theory, Methods and Applications. 2017; 287–311; DOI: 10.1016/B978-0-08-101291-8.00012-2.

5. Legrand E, Audran M, Guggenbuhl P, Levasseur R, Chalès G, Baslé MF, Chappard D. Trabecular bone microarchitecture is related to the number of risk factors and etiology in osteoporotic men. Microsc Res Tech 2007 Nov; 70(11):952-9. DOI: 10.1002/jemt.20501.

6. Silva MEB, Santos HS, Ruhland L, Rabelo GD, Badaró MM. Fractal analysis of dental periapical radiographs: A revised image processing method. Oral Surg Oral Med Oral Pathol Oral Radiol. 2023; 135(5):669–77; DOI: 10.1016/j.oooo.2022.11.014.

7. Kato CN, Barra SG, Tavares NP, Amaral TM, Brasileiro CB, Mesquita RA, et al. Use of fractal analysis in dental images: a systematic review. Dentomaxillofac Radiol. 2020; 49(2):20180457; DOI: 10.1259/dmfr.20180457.

8. Irie MS, Rabelo GD, Spin-Neto R, Dechichi P, Borges JS, Soares PBF. Use of Micro-Computed Tomography for Bone Evaluation in Dentistry. Braz Dent J. 2018; 29(3):227–38; DOI: 10.1590/0103-6440201801979.

9. Geraets WG, van der Stelt PF. Fractal properties of bone. Dentomaxillofac Radiol. 2000; 29(3):144–53; DOI: 10.1038/sj/dmfr/4600524.

10. Chappard D, Legrand E, Haettich B, Chalès G, Auvinet B, Eschard JP, et al. Fractal dimension of trabecular bone: comparison of three histomorphometric computed techniques for measuring the architectural two-dimensional complexity. J Pathol. 2001; 195(4):515–21; DOI: 10.1002/PATH.970.

11. Fazzalari NL, Parkinson IH. Fractal dimension and architecture of trabecular bone. J Pathol. 1996; 178(1):100–05; DOI: 10.1002/(SICI)1096-9896(199601)178:1<100::AID-PATH429>3.0.CO;2-K.

12. Bianciardi G. Differential Diagnosis: Shape and Function, Fractal Tools in the Pathology Lab [Internet]. Nonlinear Dynamics Psychol Life Sci. 2015 [cited 2025. Sep. 15]. Oct; 19(4):437-64. Available from: https://www.bing.com/search?qs=HS&pq=google+a&sk=CSYN1&sc=13-8&q=google+academico&cvid=e8f047b769734dcf8e96a0616f856432&gs_lcrp=EgRlZGdlKgkIABBFGDsY-QcyCQgAEEUYOxj5BzIGCAEQRRg5MgYIAhAuGEAyBggDEAAYQDIGCAQQABhAMgYIBRAuGEAyBggGEAAYQDIGCAcQRRg8MgYICBBFGDwyCAgJEOkHGPxV0gEIMjMwMmowajSoAgiwAgE&FORM=ANAB01&PC=U531.

13. Doube M, Klosowski MM, Arganda-Carreras I, et al. BoneJ: Free and extensible bone image analysis in ImageJ. Bone. 2010; 47(6):1076–79; DOI: 10.1016/J.BONE.2010.08.023.

14. Mukaka MM. Statistics corner: A guide to appropriate use of correlation coefficient in medical research [Internet]. Malawi Med J. 2012 [cited 2025. Sep. 15]. Sep; 24(3):69-71. Available from: https://pmc.ncbi.nlm.nih.gov/articles/PMC3576830/.

15. Franciotti R, Moharrami M, Quaranta A, Bizzoca ME, Piattelli A, Aprile G, et al. Use of fractal analysis in dental images for osteoporosis detection: a systematic review and meta-analysis. Osteoporos Int. 2021; 32(6):1041–52; DOI: 10.1007/S00198-021-05852-3.

16. Tomazelli KB, Bianco BC, Castro BR, Ramos I, Zimmer VR, Soares PBF, et al. Morphology and spatial distribution of cortical bone canals: Evaluation of shape parameters, lacunarity, and fractal dimension in the human irradiated mandible. Bone. 2025; 192; DOI: 10.1016/j.bone.2024.117349.

17. Chappard D, Baslé MF, Legrand E, Audran M. Trabecular bone microarchitecture: A review. Morphologie. 2008; 92(299):162–70; DOI: 10.1016/J.MORPHO.2008.10.003.

18. Araújo AS, Fernandes ABN, Maciel JVB, Netto JNS, Bolognese AN. New methodology for evaluating osteoclastic activity induced by orthodontic load. Journal of Applied Oral Science. 2015; 23(1):19–25; DOI: 10.1590/1678-775720140351.

19. van 't Hof RJ, Rose L, Bassonga E, Daroszewska A. Open source software for semi-automated histomorphometry of bone resorption and formation parameters. Bone. 2017; 99:69–79; DOI: 10.1016/J.BONE.2017.03.051.

20. Malhan D, Muelke M, Rosch S, Schaefer AB, Merboth F, Weisweiler D, et al. An Optimized Approach to Perform Bone Histomorphometry. Front Endocrinol (Lausanne). 2018; 9; DOI: 10.3389/FENDO.2018.00666.

21. Silva LM, Venâncio JF, Loures AO, Rabelo G, Lopes D, Dechichi P. Efeito do Diabetes Mellitus tipo I na organização espacial das trabéculas ósseas: análise por meio do processo de esqueletonização. HU Revista. 2019; 44(1):07–13; DOI: 10.34019/1982-8047.2018.v44.13926.